

Co-funded by the



DISCO

Grant Agreement: **755443**

DELIVERABLE **D5.5**

Development of a reactive transport model of spent fuel dissolution under near field environmental conditions.

Authors: Olga Riba, Emilie Coene, Orlando Silva and Lara Duro (Amphos 21)

Date of issue of this report: **29/03/2021**

Report number of pages: **29 p + 2 p appendices**

Start date of project: **01/06/2017**

Duration: 48 Months

Project co-funded by the European Commission under the Euratom Research and Training Programme on Nuclear Energy within the Horizon 2020 Framework Programme		
Dissemination Level		
PU	Public	X
PP	Restricted to other programme participants (including the Commission Services)	
RE	Restricted to a group specified by the partners of the Disco project	
CO	Confidential, only for partners of the Disco project	

1 Introduction and objectives

The safety assessment of deep geological repositories (DGR) of used nuclear fuel (spent fuel, SF) requires a fundamental understanding of the processes controlling fuel alteration and the release of radionuclides into the geosphere.

From the disposal concept, a reducing environment is expected at the time at which water will eventually enter in contact with the spent fuel (Puigdomenech et al, 2001). The water that may contain the fuel will be devoid of oxygen due to the corrosion of steels and cast iron in canisters, ensuring a low redox potential inside the container by the production of H_2 and Fe(II). At the same time, water radiolysis by the effect of alpha radiation (emitting gamma fission products are expected to be decayed at repository times greater than 10.000 years; when failure of the container is expected) will generate oxidizing and reducing species in solution. Taking into account that the reducing capability of H_2 is inhibited by its slow kinetics of activation, radiolysis could potentially lead to relatively fast oxidative dissolution despite the bulk reducing environment of the repository. In the last decade, several studies have shown that, as a result of the catalytic effect of epsilon particles (Rh, Pd, Ru) for the activation of hydrogen, even low hydrogen concentrations are sufficient to suppress the oxidation of UO_2 (Carbol et al, 2009; Trummer and Jonsson 2010; Ollila, 2011).

The EURATOM Project “DisCo” (modern spent fuel Dissolution and chemistry in failed Container conditions), carried out within the Horizon2020 framework program, is a collaborative effort among European partners aiming to i) advance in the understanding of the mechanisms controlling the spent fuel dissolution under repository-relevant conditions (highly reducing conditions) and ii) to fill in knowledge gaps associated with “modern” types of light water reactors (LWR) fuel, fuels doped with alumina/chromia or mixed oxide fuels (MOX). These types of fuels are increasingly being used in LWR in order to optimise reactor operation and increase energy production efficiency. The dopants trigger grain growth during sintering of the UO_2 pellets, reducing fission gas release (Arborelius et al 2012, IAEA 2010) and therefore allowing higher power rates to be achieved during reactor operation.

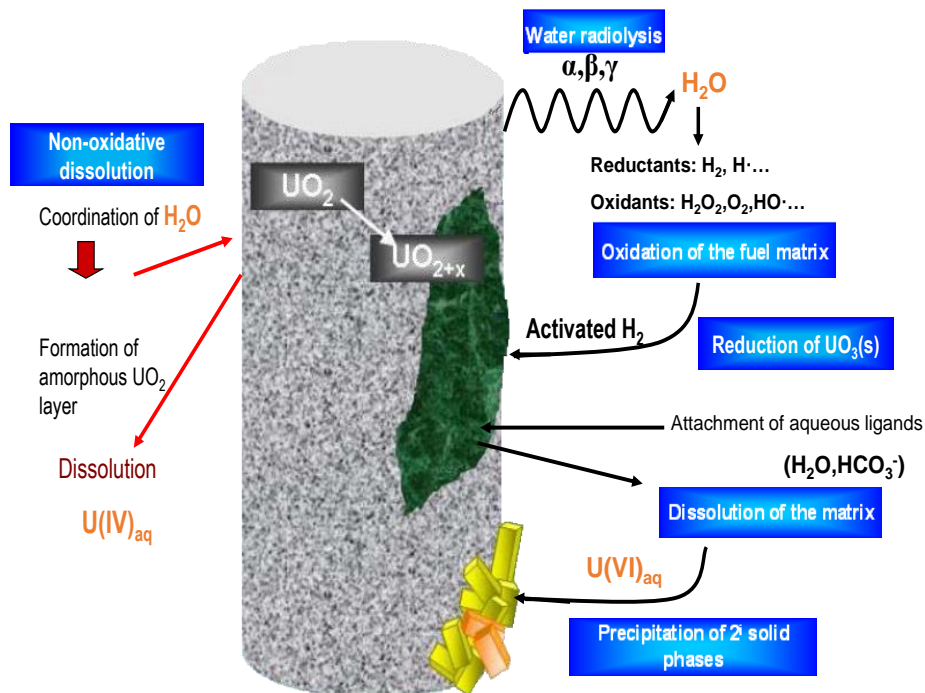
Doped fuels imply an in-reactor performance improvement, but it is not known whether the dissolution behaviour of such fuels in a geological repository environment is the same as for standard fuel. The incorporation of dopants could potentially change the electrochemical properties of the matrix and, consequently, the corrosion rate of the spent fuel matrix (He et al 2007, Razdan and Shoesmith, 2014). Therefore, while the scientific understanding of the dissolution of standard spent UO_2 fuel has reached a certain mature state (Bruno and Ewing, 2006; Ewing 2015; Shoesmith 2013), the behaviour of modern fuels under geological storage conditions is still largely unknown.

Amphos 21 has contributed to DisCo project with the development of 1D reactive transport model that has been implemented in iCP (Nardi et al. 2014). The model solves the challenge of coupling the complete water radiolysis system with chemical complexation and dissolution/precipitation reactions.

The present manuscript is structured as follows:

- i) implementation of the spent fuel matrix alteration model (MAM) (Martínez-Esparza et al., 2005) in the reactive transport tool iCP (Nardi et al. 2014), an interface coupling COMSOL Multiphysics and PhreeqC (Parkhurst and Appelo, 2013) (in section 2 and 3 of the present document)
- ii) testing the capabilities of the model by simulating new experimental data generated in the framework of DisCo project (in section 4 of the present document)
- iii) concluding remarks including a discussion on the effect of metallic dopants on spent fuel dissolution in near field environmental conditions (in section 5 of the present document)

Spent fuel is a very complex system and, as shown in Figure 1, different interrelated processes control its alteration. It is important to remark that not only hexavalent (oxidized) uranium can be released into the solution, but also tetravalent uranium can be dissolved and being predominant under reducing conditions.



Figure

Figure 1: Interrelated processes involved in the spent fuel matrix alteration (Martinez-Esparza et al., 1998)

In the literature there are currently highly advance models simulating the source-term behaviour (Duro et al., 2009; 2013; Wu et al. 2012, 2014; Jerden et al., 2015; Odorowski, 2015). The

Matrix Alteration Model (MAM) (Duro et al., 2009; 2013) is one of the most evolved radiolytic models describing the dissolution mechanism of the spent fuel matrix.

Improved models implemented in software such as COMSOL (Wu et al. 2012, 2014), MATLAB (Jerden et al., 2015), and HYTEC (Odorowski, 2015) have allowed to include the most relevant processes of the system by introducing some simplifications. These simplifications were mainly applied to the chemistry and to the radiolytic scheme. In the latter, simplifications consist of, for instance, considering only the production of H_2O_2 and H_2 instead of the complete radiolysis scheme.

2 Development of spent fuel alteration model

2.1 Evolution of the developed model

The model developed in the present study represents a step forward from the model of matrix alteration (MAM) initially development in the framework of the Spent Fuel Stability European project (2000 -2004) (Poinssot et al. 2004) as a radiolytic model with a set of kinetic processes implemented in ChemSimul (Kirkegaard and Bjergbakke, 2002). The kinetic reactions were calibrated with experimental data (Merino et al. 2005). Subsequently, in the framework of the MICADO European project (Grambow et al, 2010) and in several other projects in collaboration with ENRESA, the model was improved with the implementation of other important processes: the non-catalyzed decomposition of hydrogen peroxide, activation of H_2 by epsilon particles and the reducing effect of the activated H_2 on the oxidized surface (Duro et al. 2009; 2013).

In the framework of DisCo project, the model has been implemented in iCP (Nardi et al. 2014) and calibrated with experimental data. This implementation integrates the complete water radiolysis system and its effect on the $UO_2(am,hyd)$ alteration under container conditions. The most important feature of the described model is having solved the great challenge of: i) coupling radiolysis with reactions of chemical complexation and dissolution/precipitation processes which occur at very different time scales, often with rates differing by more than 6 orders of magnitude and ii) integrating these two systems: uranium (as the main element of the fuel) and the iron of the steel-container and metallic insert, which have a very complex chemistry.

2.2 Modelling approach

A practical method to couple water radiolysis, aqueous chemistry and solute transport was developed to simulate the dissolution of SF inside a failed waste container. The integration of the different physico-chemical processes into iCP is achieved by a two-way coupling approach, as shown in Figure 2.

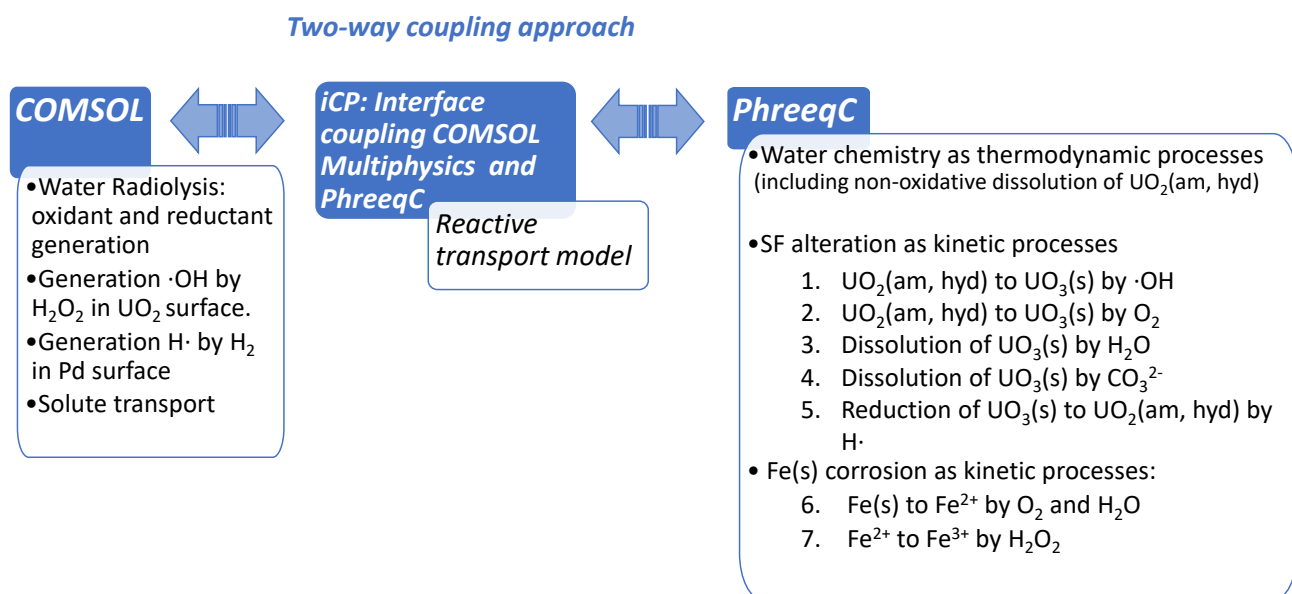


Figure 2: Integration in iCP of the different processes involved in the SF alteration.

The coupled processes included in the model are described below:

Generation of oxidants and reductants by water radiolysis with alpha/beta radiation

The present model considers the formation of radiolytic species and recombination of radiolysis products in the physico-chemical and chemical stage (Tian et al. 2017) with a set of kinetic reactions involving the following species: H^+ , OH^- , O_2 , H_2O_2 , H_2 , HO_2^- , $\text{HO}_2\cdot$, $\text{O}\cdot$, O^- , O_2^- , $\text{H}\cdot$, $\cdot\text{OH}$ and e^- . Water radiolysis by alpha and beta radiation is considered according to the treatment performed in Cera et al. (2006) and considering all the radiolytic kinetic reactions of the water scheme from Kelm and Bohnert (2004) and yields of primary products from Kelm and Bohnert (2004) and Eriksen et al. (2008) (see Appendix A).

Apart from the water radiolysis scheme, two more processes were implemented in COMSOL: the generation of $\cdot\text{OH}$ by decomposition reaction of H_2O_2 on the $\text{UO}_2(\text{am, hyd})$ surface and the generation of $\text{H}\cdot$ by activation of H_2 on the Pd surface. The kinetic constants used in the model for these two processes correspond to the values reported in Merino et al. (2005) and Trummer et al. (2008), respectively.

The generation of the above described products was implemented in COMSOL with a set of ordinary differential equations (ODE) and was coupled with the solute transport equation (Eq. 1) through a source term.

Transport of dissolved species

In theory, mineral precipitation can occur from the water that is in contact with the fuel surface. The fuel may be also considered as a porous medium. For that reason, the model considers that aqueous species are transported by diffusion according to the following equation:

$$\phi \frac{\partial c_i}{\partial t} + \nabla(-D_e \nabla c_i) = S_i + \sum_j R_{ij} \quad (1)$$

where ϕ [-] is the porosity, c_i [mol/kg_w] the aqueous concentration of species i , D_e [m²/s] the effective diffusion coefficient, S_i [mol/kg_w·s] the source term of species i and R_{ij} the reaction term between species i and j .

The chemical reaction terms S_i and R_{ij} , on the other hand, are calculated in PhreeqC as explained below (note that the radiolysis calculated in COMSOL also contributes to the source term of this equation).

Alteration of the SF surface and corrosion of Fe(s)

The solid phase considered as SF matrix is a homogeneous chemical composition of UO₂, with the formulation: UO₂(am, hyd), containing 1 atom % of Pd, as representative element of the epsilon particles. The following kinetic reactions related to the alteration of SF are implemented in PhreeqC:

1. Oxidation of UO₂(am, hyd) to UO₃(s) by ·OH
2. Oxidation of UO₂(am, hyd) to UO₃(s) by O₂
3. Dissolution of UO₃(s) by H₂O
4. Dissolution of UO₃(s) by CO₃²⁻
5. Reduction of UO₃(s) to UO₂(am, hyd) by H·

As for the oxidation of metallic Fe(s) the following kinetic processes are implemented in PhreeqC:

6. Corrosion of Fe(s) to Fe²⁺ by O₂ and H₂O
7. Oxidation of Fe²⁺ to Fe³⁺ by H₂O₂

The thermodynamic database used in the modelling is ThermoChimie version 9b0 (Giffaut et al. 2014).

2.3 Calibration of the kinetic constants

Validation of the kinetic constants of the processes 1), 2), 3), 4) and 5), occurring on the SF matrix, have been performed by comparison with the experimental data described by Cera et al. (2006). For process 6) the experimental data generated in REDUPP European project on UO₂ dissolution in natural groundwater in the presence of a corroding metallic iron strip has been used. The description of the calibration of the model is published in Riba et al. (2020).

The dissolution experiments of SF fragments reported in Cera et al. (2006), and also used in the MICADO project (Grambow et al. 2010), were set up in closed ampoules to keep the gases produced by radiolysis (O₂ and H₂). The calibration of the processes 1), 2), 3), 4) and 5),

occurring in the SF surface started with arbitrary values for the kinetic constants and they were progressively adjusted considering the experimental H_2O_2 , O_2 , H_2 and U concentrations. In a first step, only the oxidative dissolution processes were considered and the kinetic constants involved in these processes were adjusted. Afterwards, the reduction of $\text{UO}_3(\text{s})$ by $\text{H}\cdot$ (process 5) was included and its corresponding kinetic constant was calibrated.

The modelling results together with the experimental concentrations of O_2 , H_2 , H_2O_2 are shown in Figure 2a. The $[\text{U}]$ (M) obtained by Cera et al. (2006) in 2mM NaCl and in 10mM NaHCO_3 + 2mM NaCl leaching solutions is shown in Figure 2b.

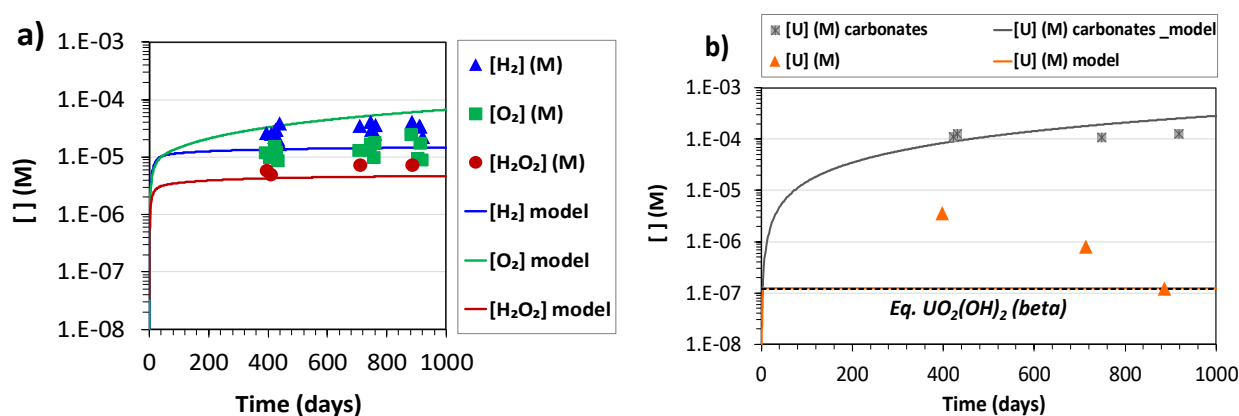


Figure 2: (a) Concentrations of H_2 , O_2 and H_2O_2 as a function of time obtained experimentally (symbols) and through the present modelling (lines); (b) concentration of U obtained experimentally by Cera et al. (2006) (symbols) and by the present modelling exercise (lines). The dashed line represents the U concentration in equilibrium with schoepite ($\text{UO}_2(\text{OH})_2(\text{beta})$).

As shown in Figure 2a, the model is well adjusted to the experimental $[\text{H}_2\text{O}_2]$. There is only a difference of less than half order of magnitude between the modelled $[\text{H}_2]$ and $[\text{O}_2]$ and the corresponding experimental data. It is worth noting that the linear dependency of $[\text{O}_2]$ with time obtained with the simulations does not follow the trend observed in the experimental data. Different tests during the calibration exercise indicated that this linear increase in the modelled $[\text{O}_2]$ is due to the radiolytic system. As a principle, it has been preferred not to adjust the kinetic constants of the water radiolysis reactions, compiled in Appendix A. As shown in Figure 2b, uranium concentration in equilibrium with schoepite ($\text{UO}_2(\text{OH})_2(\text{beta})$) has been considered to model the experiments without carbonate.

The corrosion process of metallic $\text{Fe}(\text{s})$ has been validated with experimental data generated in the frame of the REDUPP project (Zetterström Evins et al. 2014). Dissolution experiments of UO_2 α -doped with 10 atom % of ^{233}U ($31.4 \text{ MBq}\cdot\text{g}^{-1}$) and $\text{SA}/\text{V} = 12.5 \text{ m}^{-1}$ in the presence of $\text{Fe}(\text{s})$ were considered. The initial water composition corresponds to the fresh water of REDUPP experiments. However, to simplify the model only the following species were included as input data: Na^+ , Ca^{2+} , Fe^{2+} , Cl^- , HCO_3^- and SO_4^{2-} . In accordance with the experimental set up, the initial water pH and Eh were set at 8.7 and -0.39 V, respectively. Both calcite and any iron

phases included in the ThermoChimie database version 9b0 (Giffaut et al., 2014) were allowed to precipitate if they reached oversaturation. Two sets of experimental uranium concentrations in solution were used for the validation: i) total [U] (M) determined in solution and ii) calculated [U] (M) considering the isotopic composition and corresponding to uranium in solution caused by UO_2 oxidation without reprecipitation by U(VI) reduction.

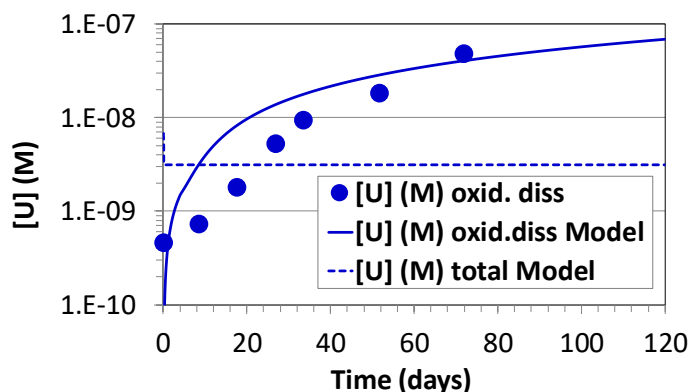


Figure 3: Symbols represent the experimental data from the REDUPP final report (Zetterström Evins et al. 2014) of UO_2 α -doped with 10 atom % of ^{233}U ; SA/V 12.5 m^{-1} , in the presence of metallic Fe(s) strip. Lines represent the modelling results of total uranium in solution (dashed line) and calculated uranium corresponding to the oxidative dissolution of UO_2 without reprecipitation (solid line).

The experimental data shown in Figure 3 is the [U] corresponding to the oxidative dissolution process for the experiments with UO_2 α -doped, 10 atom % of ^{233}U and SA/V = 12.5 m^{-1} . The calculated uranium concentration resulting from the kinetic oxidation of $\text{UO}_2(\text{s})$ by O_2 and $\cdot\text{OH}$ and subsequent dissolution with H_2O and carbonate (processes from 1) to 4) in Figure 2) (solid line in Figure 3) is in general in good agreement with the experimental data. However, the model shows an exponential increase of [U] during the first 40 days, and this pattern is not seen in the experimental data showing a linear increase instead. This initial exponential increase of [U] might be attributed to rapid generation of $[\text{O}_2]$ by water radiolysis and subsequent oxidative dissolution of $\text{UO}_2(\text{am, hyd})$. The dashed line shown in Figure 3 corresponds to the total uranium in solution calculated with the model. It corresponds to the equilibrium concentration of uranium with the $\text{UO}_2(\text{am, hyd})$ phase ([U] = $3.15 \cdot 10^{-9} \text{ M}$, in ThermoChimie database version 9b0, Giffaut et al., 2014).

Iron corrosion by H_2O and O_2 has been included in the model (process 6 in Figure 2). It is worth noting that Odorowski (2015) specifies the need of introducing a reaction accounting for the oxidation of Fe(s) under reducing conditions apart from the process of consumption of O_2 by Fe(s). First, the kinetic constant for iron oxidation in anoxic conditions was set to $6.6 \mu\text{m} \cdot \text{y}^{-1}$ in accordance with the literature under reducing conditions (Féron et al. 2008; Andra, 2005; Smart et al. 2010). Secondly, the kinetic constant for iron oxidation with O_2 was adjusted to experimental data generated in the REDUPP European project (Zetterström Evins et al. 2014) on UO_2 dissolution in natural groundwater in the presence of a corroding metallic iron strip.

The adjusted kinetic constant corresponds to a rate value of $20 \mu\text{m}\cdot\text{y}^{-1}$, which is in agreement with the values found in the literature for iron corrosion under oxidizing conditions (Féron et al. 2008). The above kinetic rate value is one order of magnitude higher than the one used by Odorowski et al. (2017) also in the DisCo project. Thus, the present simulations allow to explore a less conservative scenario, respect to the conditions studied in Odorowski et al. (2017). Finally, the kinetic constant for process 7) in Figure 2 was taken from Wu al. (2014b).

3 Results of 1D reactive transport model

After calibrating the kinetic constants, a 1D reactive transport model was implemented under reducing conditions considering a SF matrix with a homogeneous chemical composition of UO_2 (UO_2 containing 1 atom % of Pd).

A uniform alpha dose rate of $2.86 \cdot 10^{-2} \text{ Gy}\cdot\text{s}^{-1}$ affecting the first $13 \mu\text{m}$ in water adjacent to the SF surface was assumed in the 1D simulations. This uniform alpha dose rate is equivalent to a non-uniform exponential distribution of dose rate affecting $35 \mu\text{m}$ in water adjacent to the SF surface, in the sense that both produce the same total dose rate (Wu et al. 2012). The aqueous solution considered has $\text{pH} = 9$ and an initial concentration of $[\text{Fe}] = 1 \cdot 10^{-9} \text{ M}$. The production and recombination reactions of the species generated by α -water radiolysis are limited to the SF and the first $13 \mu\text{m}$ adjacent to it, whereas solute diffusion is considered in the full geometry. The right boundary allows for out-diffusion with a prescribed concentration for all solutes. From the basic described geometry and parameters, different 1D reactive transport models were implemented with the aim to study the effect of different parameters:

- i) 1D model to study the influence of Fe. In this model, the $\text{UO}_2(\text{am,hyd})$ is considered as a non-porous media and the domain length is 1 mm. The results of the simulations are presented in section 3.1.
- ii) 1D model implemented to explore the response of the geochemical system when the $\text{UO}_2(\text{am,hyd})$ is assumed to be a porous medium and Fe is present in the system as a small domain (1 micra of length). The results are presented in section 3.2.1.
- iii) 1D model implemented to evaluate a geometry closer to the investigated system of spent fuel rods in a distance of 9 mm to iron materials. In this last simulation, $\text{UO}_2(\text{am,hyd})$ is considered as a porous medium, as in the previous simulation, and the iron domain length is increased to 1mm. The results are presented in section 3.2.2.

3.1 1D reactive transport model with $\text{UO}_2(\text{am,hyd})$ as a non-porous medium

The following two 1D simulations were run to quantify the effect of Fe on the alteration of spent fuel:

- i. **Simulation without Fe(s)**, where the model considers three sub-domains: SF surface zone ($1 \mu\text{m}$), α -radiation zone in the water very close to the SF surface ($13 \mu\text{m}$) and a diffusion zone being considered in the full geometry (1 mm).

- ii. **Simulation with Fe(s)**, where the model considers four sub-domains: the same three domains described in *simulation without Fe(s)*, plus a steel surface zone (1 μm), which composition correspond to 99% of Fe.

To compare with existing simulations, the models consider the same parameters and geometry as in Wu et al. (2012). For that reason, the extension of the domain was assumed to be 1 mm (Figure 4). The concentration at the right boundary is prescribed to zero for all species except for Fe in the second simulation. Both models include a non-porous SF matrix surface at the left boundary. This surface is closed to solute transport but interacts chemically with water in the Spent Fuel matrix surface zone (see Figure 4). Porosity is set to 1 in the whole model resulting in an effective diffusion coefficient of $10^{-9} \text{ m}^2/\text{s}$ for all species.

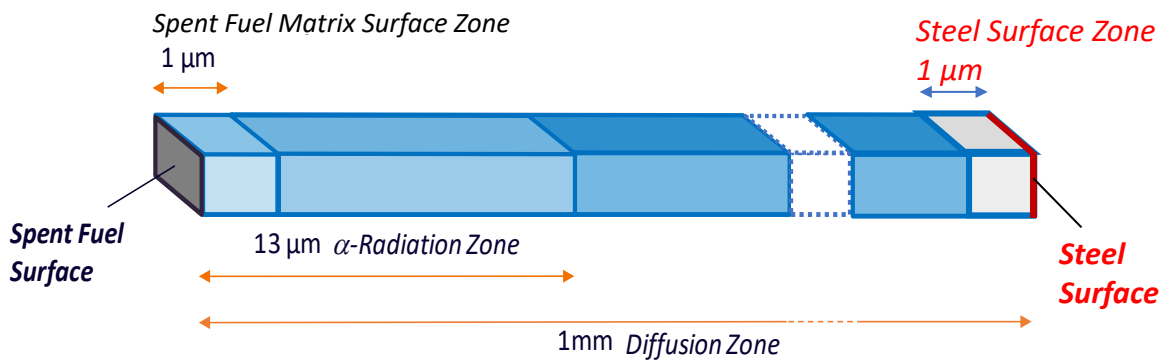


Figure 4: Geometry (not to scale) considered in the 1D model with $\text{UO}_2(\text{am,hyd})$ as a non-porous medium to simulate the processes occurring in the spent fuel matrix surface described in Figure 1.

The calculated concentrations of the species generated by water radiolysis (H_2O_2 , $\text{O}_2(\text{aq})$, $\text{H}_2(\text{aq})$, $\text{H}\cdot$, $\cdot\text{OH}$, e^- , $\text{HO}_2\cdot$, O^- , $\text{O}\cdot$, HO_2^- and O_2^-) reached steady state very rapidly (in 4 hours). On the other hand, the concentration of uranium increases progressively reaching a quasi-steady state after 36.5 days.

The concentrations of H_2O_2 , $\text{O}_2(\text{aq})$, $\text{H}_2(\text{aq})$ and U as a function of the distance from the SF surface at 36.5 days are shown in Figure 5a (for the simulation without Fe) and Figure 5b (for the simulation with Fe). It is observed that H_2O_2 , $\text{O}_2(\text{aq})$ and $\text{H}_2(\text{aq})$ stabilized at similar concentrations in both cases. Nonetheless, the total uranium concentration is $\sim 10^{-9} \text{ M}$ in the absence of Fe and it is mainly in the oxidized form U(VI) ($\sim 80\%$ of total uranium). This is consistent with the fact that the redox pair U(IV)/U(VI) controls the $\text{Eh} = -0.2 \text{ V}$ at $\text{pH} = 9$ (see Figure 5c). However, for the simulation with Fe(s), the uranium in solution predominates in its reduced form. This is associated to an $\text{Eh} = -0.4 \text{ V}$ at $\text{pH} = 9$, controlled by the redox pair $\text{Fe}^{2+}/\text{magnetite}$, with $[\text{Fe}]_{\text{total}} = 10^{-8} \text{ M}$, as shown in Figure 5c.

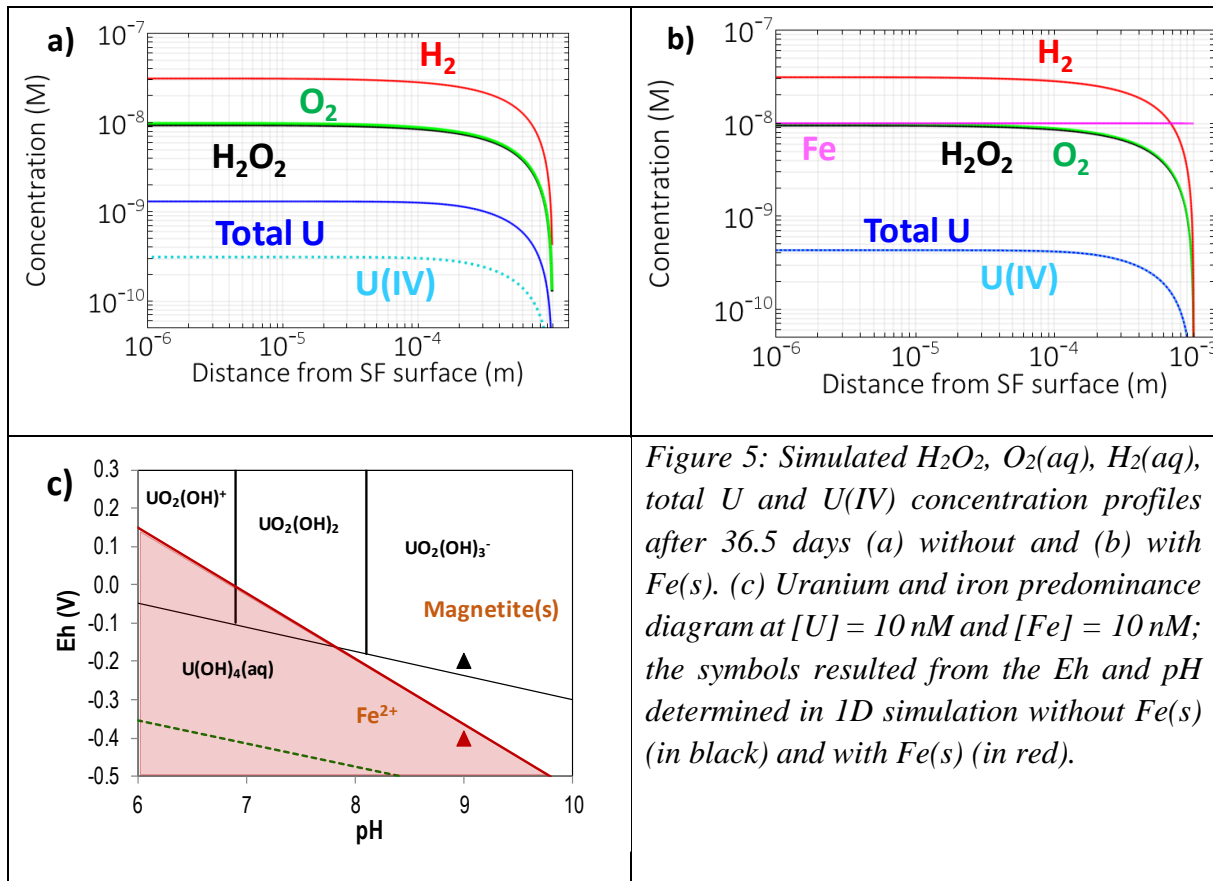


Figure 5: Simulated H_2O_2 , $O_2(aq)$, $H_2(aq)$, total U and U(IV) concentration profiles after 36.5 days (a) without and (b) with Fe(s). (c) Uranium and iron predominance diagram at $[U] = 10 \text{ nM}$ and $[Fe] = 10 \text{ nM}$; the symbols resulted from the Eh and pH determined in 1D simulation without Fe(s) (in black) and with Fe(s) (in red).

The obtained results are comparable with the concentrations simulated in Wu et al. (2014b), calculated under the same alpha dose rate and radiation range in water. The concentrations of $H_2(aq)$, H_2O_2 and U are very similar in both models. However, the $O_2(aq)$ concentration is almost two orders of magnitude higher in the present model than in Wu et al. (2014b). Our kinetic constants were calibrated against experimental data from Cera et al (2006) and this gives confidence to the results obtained in this work. The difference between the O_2 concentrations in Wu et al. (2014b) and those in the present model can be attributed to the different radiolytic schemes and the different reaction rates or processes considered in the SF matrix by each model. The $UO_2(am,hyd)$ dissolution rate determined from the present model without Fe(s) is $2 \cdot 10^{-6} \text{ y}^{-1}$ ($1.2 \text{ pmol} \cdot \text{m}^{-2} \cdot \text{s}^{-1}$) which is in the range of the values considered in safety assessments (10^{-7} y^{-1} , with maximum = 10^{-6} y^{-1} and minimum = 10^{-8} y^{-1}) (Martínez Esparza, 2005; SKB, 2010; POSIVA, 2013; Johnson, 2014; NWMO, 2015; JAEA, 2015). The above occurs when the inhibiting (protecting) effect of H_2 on the long-term dissolution of SF matrix is considered. Including iron in the model reduced the corrosion rate down to 10^{-6} y^{-1} ($0.6 \text{ pmol} \cdot \text{m}^{-2} \cdot \text{s}^{-1}$). This limited effect of Fe on the alteration of the SF matrix alteration may be due to the small surface area of the steel considered in the model. However, it should be noted that Wu et al. (2014b) showed that when the Fe^{2+} concentration in the bulk solution increased from 0 to 10^{-8} M , the diffusive flux of UO_2^{2+} decreased only from 0.6 to $0.5 \text{ pmol} \cdot \text{m}^{-2} \cdot \text{s}^{-1}$. This is associated to a reduction in the SF dissolution rate of only 20%, which is in the same order of magnitude than the reduction predicted with the present simulations.

3.2 1D reactive transport model with UO₂(am,hyd) as a porous medium

To quantify the effect of porosity on the dissolution of the spent fuel matrix a porous UO₂ containing 1 atom % of Pd was considered in the model. The porosity is set at 0.15, a value estimated by considering a density of 8.93 g/cm³ for a porous UO₂ pellet (Cobos et al. 2019) and a grain density of 10.52 g/cm³ (Arborelius et al. 2006). The estimated porosity is equivalent to a specific surface area of 21.3 m²/mL (in comparison with 1 m²/mL used in the simulations described in section 3.1). The following two 1D simulations were performed for different geometry dimensions. The first simulation, named *synthetic configuration*, is described in section 3.2.1 and considers the same steel surface zone dimensions (1 μm) and distance between the pellet surface and the steel surface (1mm) as the simulation described in section 3.1. The second simulation, named *configuration representative of a DGR*, is presented in section 3.2.2 and considers dimensions that are more representative of the expected design in a DGR.

The model of the porous SF is shown in Figure 6 and considers four sub-domains: a porous SF matrix zone, an α-radiation zone in the water adjacent to the SF surface, a diffusion zone, and a steel surface zone. The steel surface zone is assumed to be pure water (porosity = 1) in contact with a steel surface. The dimensions considered in these simulations are presented in Table 1. For both configurations, the length of the α-radiation zone is 13 μm.

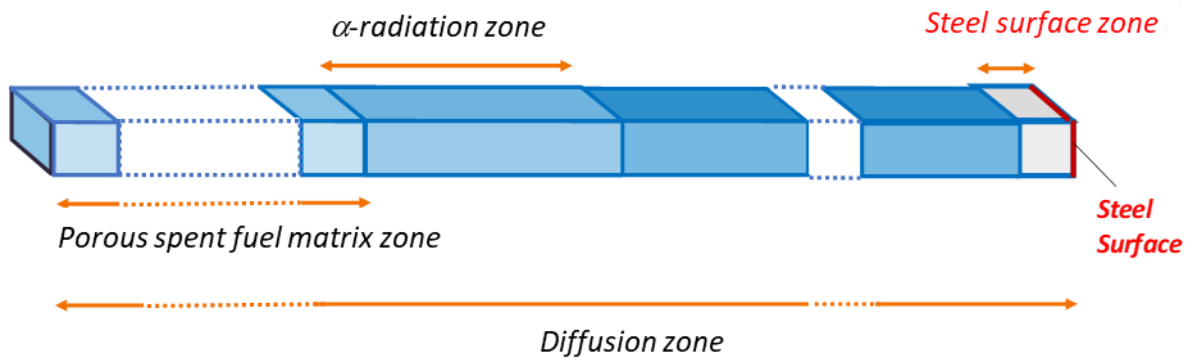


Figure 6. Geometry (not to scale) of the 1D model considering a porous spent fuel matrix.

Table 1. Configurations studied with the 1D model (see Figure 6) considering a porous spent fuel matrix.

Zone	Synthetic configuration	Configuration representative of a DGR
Porous spent fuel matrix	5 mm	4 mm
Diffusion	6 mm	14 mm
Steel surface	1 μm	1 mm
α-radiation	13 μm	13 μm

3.2.1 Synthetic configuration

Figure 7a presents the evolution of total U and U(IV) concentration profiles in solution. The simulated U concentration agrees with precipitation of schoepite ($\text{UO}_2(\text{OH})_2(\text{beta})$) inside the pellet (seen in Figure 7b) limiting the uranium in solution to $[\text{U}] = 5 \cdot 10^{-7} \text{ M}$ at $E_h = -0.16 \text{ V}$ (ThermoChimie database version 9b0, Giffaut et al., 2014). Inside the SF and close to the interface with the free aqueous phase, the uranium decreases sharply with $[\text{U}] = 6 \cdot 10^{-8} \text{ M}$ at the surface after 34 days. A front of U(VI)(aq) starts forming in the free aqueous phase at the interface with the $\text{UO}_2(\text{am,hyd})$ surface, being significant at 3 days. This front increases and moves away from the $\text{UO}_2(\text{am,hyd})$ surface until it reaches a steady state after 29 days at a maximum distance of ~ 500 microns away from the SF pellet surface. Nearby the Fe(s) surface (right boundary), the total uranium in solution is U(IV)(aq) in equilibrium with $\text{UO}_2(\text{am,hyd})$ and the $E_h = -0.4 \text{ V}$. Note that the existence of this oxidized U(VI)(aq) front might be conditioned by the small size of the steel surface. The estimated corrosion rate calculated with the present simulation is $9 \cdot 10^{-7} \text{ y}^{-1}$, similar to the simulation discussed in section 3.1 when a steel surface zone is considered.

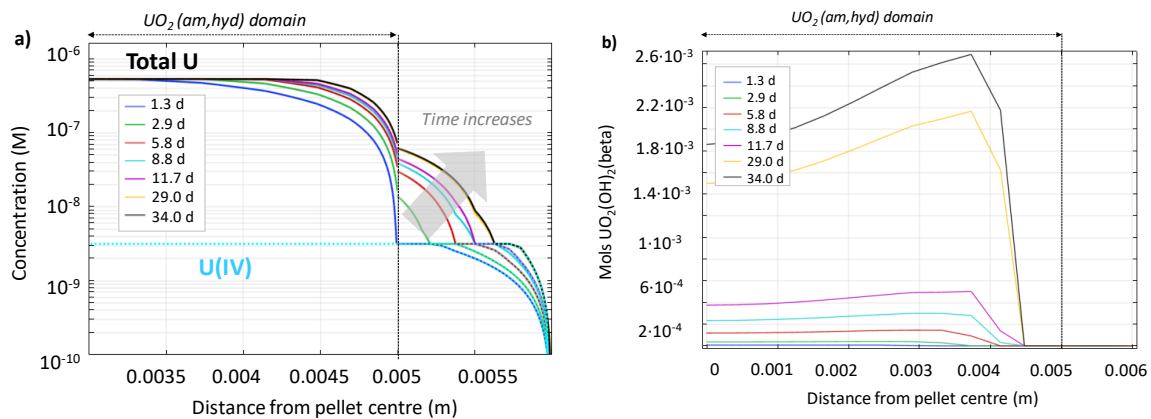


Figure 7. Modelling results considering the geometry detailed in Figure 6 and Table 1 for a synthetic configuration. (a) Total U (solid lines) and U(IV) (dotted lines) concentration profiles at different simulation times. (b) Moles of schoepite at different simulation times.

3.2.2 Configuration representative of a DGR

A new 1D reactive transport simulation has been performed with a geometry considering dimensions that are more representative of the expected design in a DGR. The geometry in this 1D simulation (see Figure 6 and Table 1) represents the canister design of shell made of copper and a mechanical load-bearing nodular cast iron insert in which the spent fuel is placed for final disposal in the repository (Raiko 2012).

Figure 8a presents the evolution of total U and U(IV) aqueous concentration profiles. The results show that, due to oxidation of the matrix, $[\text{U}]$ increases quickly between 12 and 29 days. From 34 days, $[\text{U}]$ reaches a value of $5 \cdot 10^{-7} \text{ M}$ corresponding to the equilibrium with schoepite ($\text{UO}_2(\text{OH})_2(\text{beta})$) precipitating at the pellet centre. Away from the pellet centre, the total $[\text{U}]$ in the solution corresponds to $[\text{U(IV)}]_{\text{aq}}$ in equilibrium with $\text{UO}_2(\text{am,hyd})$ until the end of the

simulation (37 days). In the bulk of the solution, the $[U(IV)]_{aq}$ progressively decreases from $3 \cdot 10^{-9} M$, in equilibrium with $UO_2(am,hyd)$, to zero, which is reached at $10^{-5} m$ from the iron surface. As can be observed in Figure 8b, the $[U]$ profile is consistent with the formation of Fe^{3+} and the evolution of Eh of the system. Coinciding with the increase of total U concentration, the Eh sharply increases to $-0.16V$ at the pellet centre, from $-0.48V$ in the bulk of the solution.

As has already been pointed out at the end of the discussion in section 3.2.1 in relation to the effect of iron on the SF alteration, this simulation confirms that increasing the steel surface zone from a length of $1 \mu m$ to $1 mm$, results in a substantial decrease of the oxidation front of the spent fuel matrix (compare Figure 8a and Figure 7a). Also, the start of oxidation is delayed, and its duration limited to 5 days (from day 29 to day 34), in contrast to what occurs in the previous simulation in which SF oxidation is observed from day 1.

The estimated corrosion rate calculated with the present simulation is $2 \cdot 10^{-7} y^{-1}$ significantly lower than the values calculated from the models with a steel surface zone of $1 \mu m$ (simulations discussed in sections 3.1 and 3.2.1).

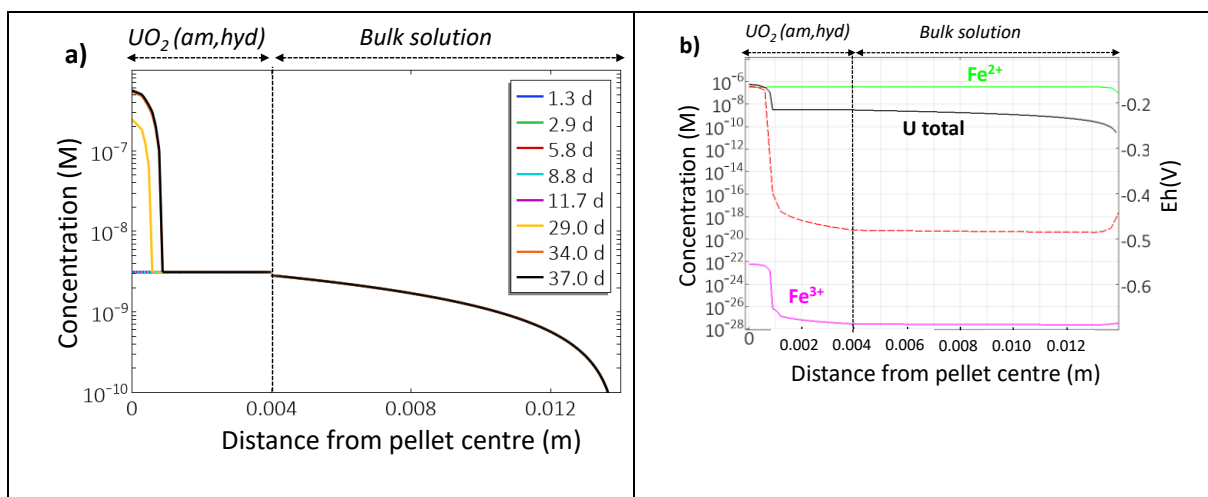


Figure 8. Modelling results considering the geometry detailed in Figure 6 and Table 1 for a configuration representative of a DGR (a) Total U (solid lines) and U(IV) (dotted lines) concentration profiles at different simulation times. (b) Concentration of Fe^{2+} (green line), Fe^{3+} (magenta line) and total U (black line), and Eh(V) (red dotted line) in the secondary “y” axis, at 36.5 days simulation time.

4 Simulation of experiments performed in the DisCo project

The model has been applied to simulate independent experimental data (not used in the calibration of the kinetic constants) generated in WP3 and WP4 of DisCo. The following leaching experiments performed in carbonated water have been simulated:

- i) Standard UO_2 spent fuel leaching experiments, from Studsvik Nuclear AB.

- ii) Unirradiated Cr-doped UO_2 and Al-Cr-doped UO_2 leaching experiments, from CIEMAT.
- iii) Unirradiated pure UO_2 leaching experiments in presence of hydrogen peroxide, from JÜLICH.

4.1 Simulation of standard UO_2 spent fuel leaching experiments performed at Studsvik Nuclear AB

The standard UO_2 spent fuel leaching experiments performed in Studsvik Nuclear AB are described in Fidalgo et al. (2020). In these experiments, the fuel was irradiated in a commercial boiling water reactor to a local burnup of ~ 51.7 MWd/kgU. After a washing step to eliminate any pre-oxidized phases formed during air storage in cell, the fuel fragments were leached in a synthetic groundwater (consisting of 10 mM NaCl and 2 mM NaHCO_3 and stabilizing a pH = 8.2). An autoclave pressurized up to 55 bar of H_2 was used (no replenishment of gas due to pressure loss during the experiment was performed to avoid air intrusion in the system). Figure 9 shows the evolution of the experimental concentrations of ^{237}Np (a), ^{99}Tc (b), ^{239}Pu (c), ^{100}Mo (d) and Figure 10a, the measured concentration of ^{238}U (black dots).

When applying the spent fuel matrix alteration model to simulate the above experiment, the following calculations and considerations were made:

- i. The dose rate was calculated for the UO_2 spent fuel fragments from the radioisotopes inventory detailed in First Nuclides European project (Roth et al. 2014). This was used to determine the temporal evolution of oxidants and reductants.
- ii. The specific surface area is a parameter often affected by uncertainties. However, some test simulations showed that it is not a very sensitive parameter and an increase of 50% in the specific surface area does not change the results significantly. The rates for the oxidation processes (processes 1 and 2 in Figure 2), were implemented considering a specific surface of $4.6 \text{ cm}^2/\text{g}$. This value was calculated considering a roughness factor of 3 and averaging two surface area values calculated assuming the fragments have: i) a cubic geometry and ii) a sphere geometry.

The selected equilibrium phases limiting the solubility of ^{237}Np , ^{99}Tc , ^{239}Pu , and ^{100}Mo are $\text{NpO}_2 \cdot 2\text{H}_2\text{O}(\text{am})$, $\text{TcO}_2 \cdot 1.6\text{H}_2\text{O}$, $\text{PuO}_2(\text{coll})$ and $\text{MoO}_2(\text{s})$, respectively. The dashed lines shown in Figure 9 represent the equilibrium concentration of these phases calculated with the equilibrium constants available in the ThermoChimie database version 9b0 (Giffaut et al. 2014). The selection of the most likely limiting phases was made by considering that the system is approaching a steady state and taking the concentrations at 741 days as a reference.

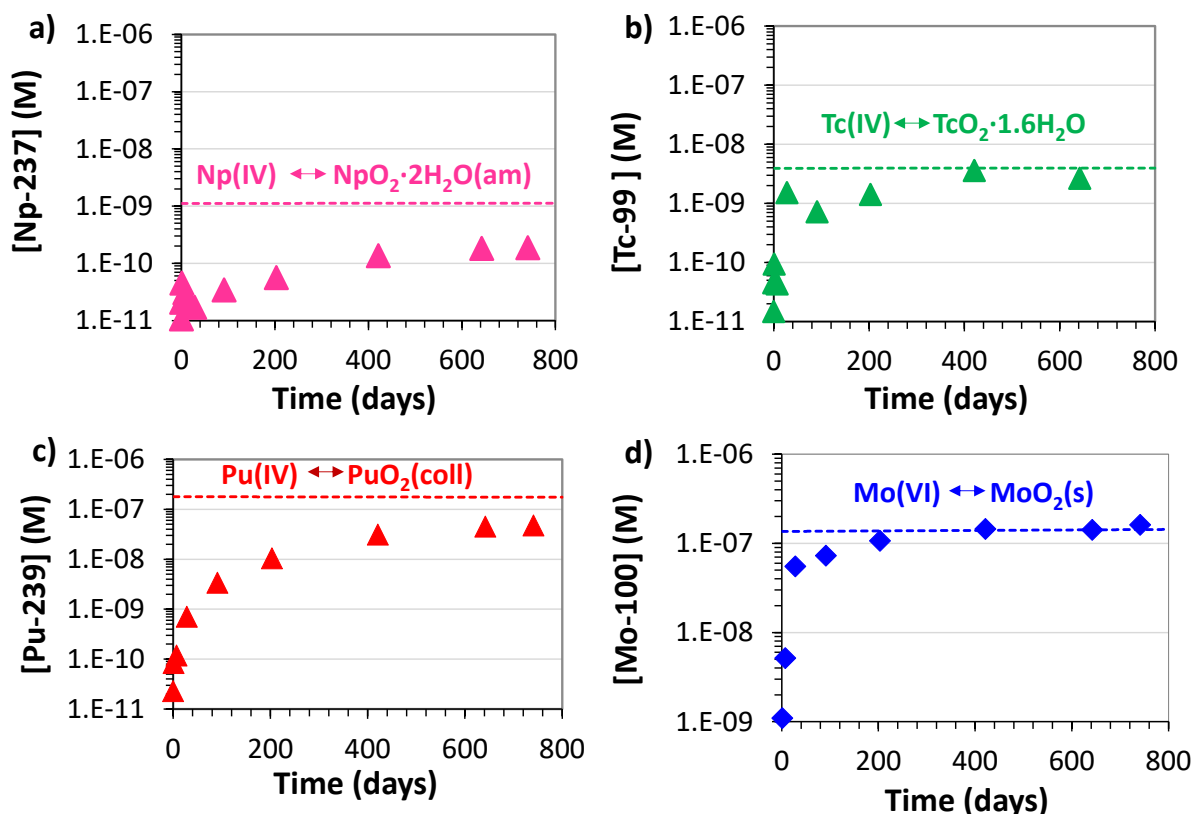


Figure 9: Measured concentrations of (a) ^{237}Np , (b) ^{99}Tc , (c) ^{239}Pu and (d) ^{100}Mo as function of time taken from Fidalgo et al. (2020), represented as symbols. The dashed lines indicates the equilibrium concentrations of each element considering as limiting phases $\text{NpO}_2\cdot 2\text{H}_2\text{O}(\text{am})$, $\text{TcO}_2\cdot 1.6\text{H}_2\text{O}$, $\text{PuO}_2(\text{coll})$ and $\text{MoO}_2(\text{s})$, respectively.

Under the simulated conditions described above, the Eh stabilizes at -0.3 V . As indicated in Figure 10c, it seems that the redox pair $\text{MoO}_4^{2-}/\text{MoO}_2$ is controlling the Eh of the system.

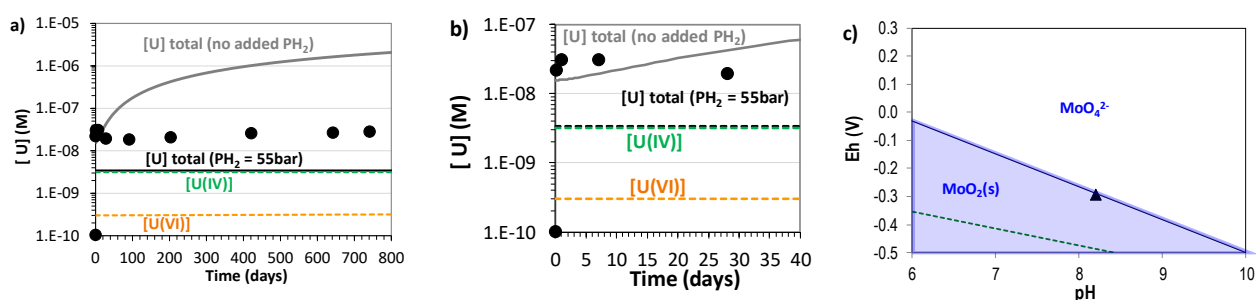


Figure 10: (a) Measured concentrations of ^{238}U as function of time taken from Fidalgo et al. (2020), represented as symbols. Simulated concentrations are represented by dashed lines for total U (black), U(IV) (green) and U(VI) (orange) at $\text{PH}_2 = 55\text{ bar}$. The solid grey line represents the total [U] when no $\text{H}_2(\text{g})$ is added. (b) Zoom in of Figure (10a). (c) Molybdenum predominance diagram $[\text{Mo}]_{\text{total}} = 1\cdot 10^{-7}\text{ M}$, the symbol corresponds to the Eh and pH determined with the model.

Figure 10(a and b) presents the uranium in solution determined experimentally by Fidalgo et al. (2020). In these figures, the total uranium concentration calculated with the model

considering a $P_{H_2} = 55$ bar is represented by dashed black lines. The total uranium concentration simulated with only the hydrogen generated by radiolysis (no added H_2 pressure) is represented by the grey solid line. The experimental uranium concentration increases during the first day reaching a maximum concentration of $\sim 3 \cdot 10^{-8}$ M, as shown in Figure 10b. The model with no added P_{H_2} is close to the experimental data during this short period. Subsequently, the experimental $[U]$ decreases slightly until $\sim 2 \cdot 10^{-8}$ M and then, from the day 100, it starts to increase again at a very slow rate reaching a concentration of $3 \cdot 10^{-8}$ M after 741 days. This concentration is about one order of magnitude higher than the solubility of amorphous $UO_2(am, hyd)$ (see Figure 10a). At reaction times > 30 days, the simulated $[U]$ with no added P_{H_2} displays a linear increase, reaching values of $\sim 10^{-6}$ M at 400 days. On the other hand, the model considering $P_{H_2} = 55$ bar results in total $[U] = 4 \cdot 10^{-9}$ with 8% of this total uranium in the oxidized form. Therefore, the simulated uranium is predominantly $[U(IV)](aq)$ in equilibrium with $UO_2(am, hyd)$. The simulated uranium concentration is about one order of magnitude lower than the experimental values. This supports the hypothesis of Fidalgo et al. (2020) that pre-oxidized phases, presumably formed during humid storage of the spent fuel, have conditioned the release of the uranium in solution.

4.2 Simulation of unirradiated Cr-doped UO_2 and Al-Cr-doped UO_2 leaching experiments performed at CIEMAT

The present model has been applied to simulate the dissolution of Cr and Al-Cr doped UO_2 in bicarbonate water (0.019M $NaHCO_3$ and 0.001M $NaCl$). The uranium oxide pellets were synthesized in CIEMAT from UO_2 purified powder. The characterization of the sample indicated the formation of a single and pure free phase caused by surface oxidation. The leaching experiments were performed in an autoclave under 7-8 bar of 4.7% H_2/N_2 , at pH = 8.9 buffered by bicarbonate water and the reactants were prepared inside a glove box under an initial Ar atmosphere (oxygen intrusion was detected with $[O_2] = 1000$ ppm). A more detailed description of the experimental procedure is published in Rodríguez-Villagra et al. (2020). The evolution of uranium concentration with time for Cr doped UO_2 and Al-Cr doped UO_2 is shown in Figure 11.

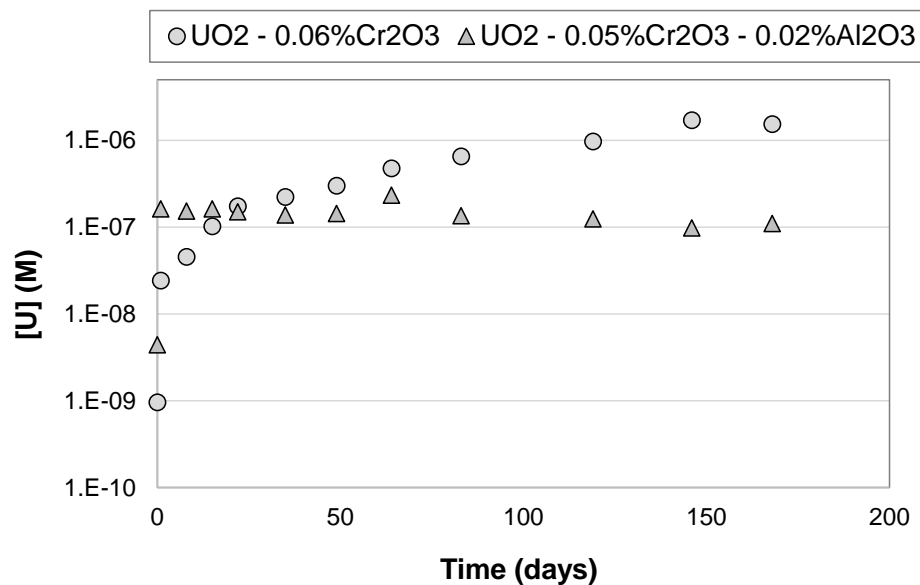


Figure 11: Measured concentrations of ^{238}U as function of time from Rodríguez-Villagra et al. (2020), represented as symbols. Circles represent data from UO_2 doped with 0.06% Cr_2O_3 and triangles represent data from UO_2 doped with 0.05% Cr_2O_3 – 0.02% Al_2O_3 .

The uranium temporal evolution for the two different doped UO_2 pellets indicate a different behaviour despite that both leaching experiments have followed the same experimental procedure with a hydrogen atmosphere of $P_{\text{H}_2} = 0.37\text{atm}$. While UO_2 doped with 0.06% Cr_2O_3 results in an exponential trend with an increase of aqueous uranium with time, in the UO_2 doped with 0.05% Cr_2O_3 – 0.02% Al_2O_3 experiment, uranium reaches a plateau at $\sim 10^{-7}$ M from the beginning of the experiment.

The two leaching experiments were simulated in PhreeqC without considering water radiolysis and assuming that:

- The leaching bicarbonate water was in equilibrium with a O_2 partial pressure of 0.001 atm (in accordance with the detected O_2 concentration in the glove box where the leaching solution was prepared).
- The kinetic processes considered were those previously calibrated (see section 2.3): the oxidation of UO_2 surface by O_2 and subsequent dissolution of oxidized surface by H_2O and carbonate (processes 2, 3 and 4 in Figure 2). Also, in both cases it was studied the possibility of H_2 being activated on Cr surface and the subsequent reduction of oxidized uranium by activated H_2 (process 5 in Figure 2).
- The kinetic constant considered for the activation process of H_2 in Cr_2O_3 was $10^{-6} \text{ m} \cdot \text{s}^{-1}$. This rate was determined in Trummer et al. (2008) for the activation of H_2 with palladium and was identified to be controlled by diffusion.
- The ratio surface area / volume of solution considered in the simulation for the kinetic processes of UO_2 oxidation by oxygen and UO_3 reduction by $\text{H} \cdot$ (processes 2 and 5 in Figure 2), respectively, was calculated from the geometry of the pellet and considering a roughness factor of 3.5 (Iglesias and Quiñones, 2008). The upper limit of the

roughness factor, 9, was also considered in the simulations (Iglesias and Quiñones, 2008).

- The ratio surface area / solution volume considered in the activation of H₂ with Cr₂O₃ was calculated with the mass fraction of Cr₂O₃ contained in the pellets.
- The value of the density of sites for UO₂ considered in the simulations was experimentally determined from the maximum Cs sorption on the UO₂ surface, assuming a site density = $1.76 \cdot 10^{-4} \text{ mol} \cdot \text{m}^{-2}$ (Rodríguez-Villagra et al. 2016, 2017). This value is close to the value calculated by Clarens et al. (2003) and used in the other simulations discussed in the present document.

With the above considerations, two types of simulations have been performed and the results are presented in Figure 12.

- a) H₂ not activated: the simulations considering that the Cr₂O₃ contained in the pellets is not able to activate H₂ are represented as blue lines in Figure 12a and 12b. Assuming a surface roughness factor of 3.5 for the calculation of the pellet surface area (Iglesias and Quiñones, 2008), the simulation results indicate the model fits the uranium released in the leaching experiment of UO₂ doped with 0.06% Cr₂O₃ fairly well. The same model is improved if a surface roughness factor of 9 is used in the simulation and, in the long-term, agrees with the simulation considering the oxidation of the UO₂ by O₂ being controlled by thermodynamic equilibrium (Figure 12a). However, the same simulation but applied to the pellet UO₂ doped with 0.05% Cr₂O₃ – 0.02% Al₂O₃ (in terms of pellet dimensions, pellet weight and amount of Cr₂O₃) does not fit the trend of the experimental data, which reach a plateau at the beginning of the leaching experiment (Figure 12b).
- b) H₂ activated: the simulations considering that Cr₂O₃ contained in the pellets activates H₂ are represented by red lines in Figure 12a and 12b. Considering a surface roughness factor of 3.5 (Iglesias and Quiñones, 2008), the simulated concentrations match well the uranium released in the leaching experiments of UO₂ doped with 0.05% Cr₂O₃ – 0.02% Al₂O₃ (Figure 12b).

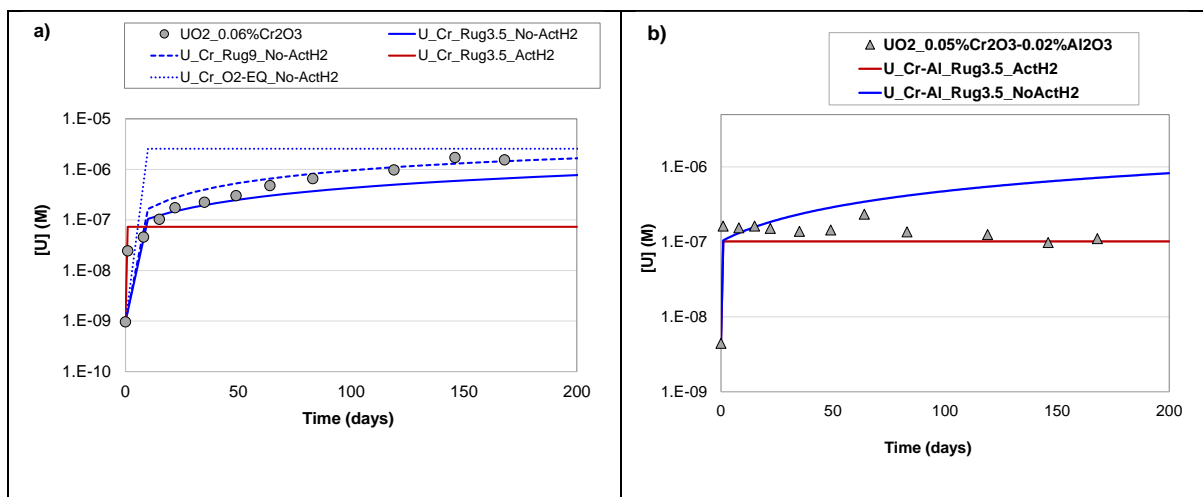


Figure 12: Measured concentrations of ^{238}U (symbols) as function of time from Rodríguez-Villagra et al. (2020), compared with the simulated concentrations (lines). a) UO_2 doped with 0.06% Cr_2O_3 and b) UO_2 doped with 0.05% Cr_2O_3 – 0.02% Al_2O_3 . Red and blue lines represent simulation results with and without H_2 activated by Cr_2O_3 , respectively. Solid lines correspond to a surface roughness factor of 3.5; dashed line is for a surface roughness factor of 9 and dotted line represents UO_2 oxidation by O_2 in thermodynamic equilibrium.

Therefore, the simulation of the above two types of behaviour observed in the leaching experiments suggests that Cr_2O_3 supported by Al_2O_3 can activate H_2 but this capability is diminished for non-supported Cr_2O_3 particles. This result agrees with the results found in the study of the different catalytic activity between Cr_2O_3 and Cr_2O_3 - Al_2O_3 in the oxidative deshydrogenation used in the production of alkenes (Cherian et al. 2002, Jibril et al. 2005; Romero et al. 1996). When chromia is supported on another metal oxide (e.g. Al_2O_3 , TiO_2 , SiO_2 , ZrO_2 , etc.), the structure and reactivity properties are altered by stabilization of Cr in different oxidation states (Cr^{3+} , Cr^{5+} and Cr^{6+}) and an improvement in the activity/selectivity of these chromia-based catalysts is observed (Sohn and Ryu 1993, Scharf et al. 1994, Józwiak and Dalla Lana 1997, Zaki et al. 1998).

4.3 Simulation of unirradiated pure UO_2 and Cr-doped UO_2 leaching experiments in presence of hydrogen peroxide performed at JÜLICH

The present model was applied to simulate the dissolution of pure UO_2 and Cr-doped UO_2 in 10 mM of NaHCO_3 and 2.25 mM H_2O_2 , to mimic the oxidative dissolution of UO_2 . The detailed description of the experimental procedure is published in Kegler et al. (2020). Briefly, the uranium oxide pellets, synthesized in JÜLICH in the framework of WP2, were leached in anoxic solution conditions achieved by flushing with Ar during the complete experimental run time. Figure 13 shows the evolution of uranium concentration with time in the leaching experiments of UO_2 reference pellets (Exp. 1 to 5) and Cr-doped UO_2 pellets (Exp. 6 to 10). The concentrations of U are normalized by the geometrical surface area of the pellet. As discussed in Kegler et al. (2020), the slightly higher initial dissolution rate of pure UO_2 compared to Cr-doped UO_2 pellets (Figure 13), can be explained by the slightly lower density of pure UO_2 pellets (porosity varying between 3.5% and 6.5%) in comparison with the porosity

of Cr-doped UO_2 pellets, that ranges between 1.25% and 3.8%. As stated in Kepler et al. (2020), the uranium concentration is normalized with the geometrical surface area and not to the real available reactive surface area of the pellets.

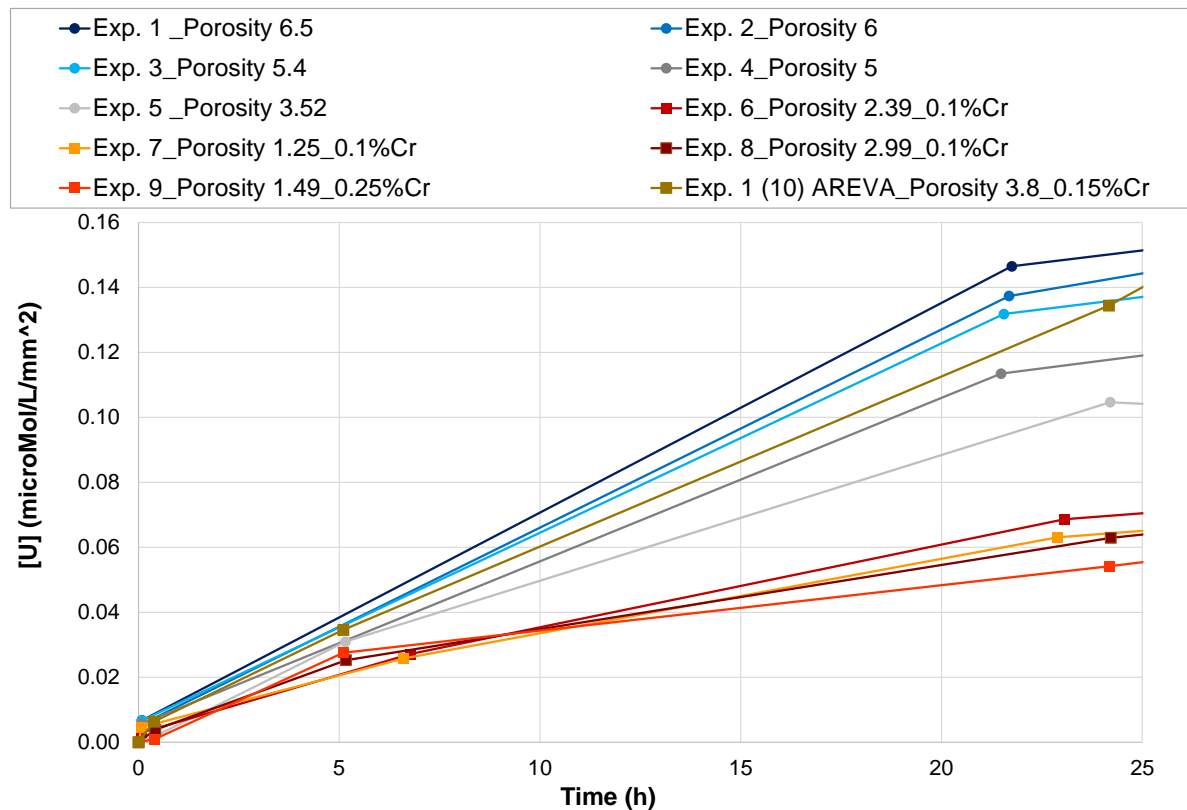


Figure 13. Normalized uranium concentration as function of time measured in leaching experiments with pure UO_2 pellets (Exp 1 to 5) and Cr-doped UO_2 pellets (Exp. 6 to 10, from Kepler et al. (2020)). Measured porosity (%) of each pellet is specified in the legend.

The leaching experimental data from the different experiments were simulated with the present model (labelled as *model-Ref*) considering the following assumptions:

- H_2O_2 added in the solution is decomposed on the surface of the UO_2 pellet to generate the radical hydroxyl ($\cdot\text{OH}$), as previously discussed and considering the rate constant reported in Merino et al. (2005).
- Oxidation of UO_2 by $\cdot\text{OH}$ following kinetic process 1 (Figure 2) included in the present model and subsequent dissolution (processes 3 and 4 in Figure 2).
- The ratio surface area / volume solution considered in the simulations was calculated from the geometry of the pellet dimensions and a roughness factor of 3.5 (Iglesias and Quiñones, 2008).

The simulation results obtained for Exp. 2 with the above-described considerations are shown in Figure 14. A good fit is found between the measured and simulated decomposition rate of H_2O_2 (compare solid orange line and symbols in Figure 14b). However, the model overestimates the dissolution of UO_2 pellet in about two orders of magnitude (compare solid blue line and symbols in Figure 14a).

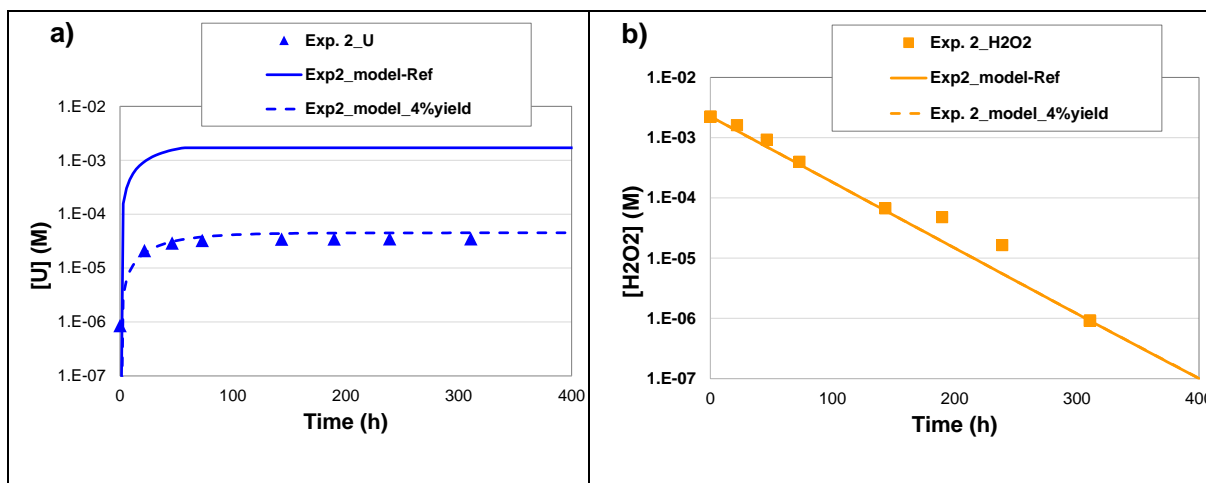


Figure 14. Symbols represent the temporal evolution of the measured (a) $[U]$ and (b) $[H_2O_2]$ in the leaching Exp. 2 using a pure UO_2 pellet (Kegler et al., 2020). Lines represent the results of the simulation.

The overestimation of the $[U]$ with the *model-Ref* suggests that only certain amount of the produced $\cdot OH$ is available for the oxidation of UO_2 due to species acting as $\cdot OH$ scavenger (HCO_3^- and H_2O_2) (Barreiro et al. 2018). The yield of this oxidation process has been quantified around 80% in UO_2 powder leaching experiments (Jonsson et al. 2003). However, the yield is much lower when considering doped (UO_2/Y_2O_3 , UO_2/Pd ; SIMFUEL) and undoped UO_2 pellets (Barreiro et al., Pehrman et al. 2012; Nilsson et al. 2011; Lousada et al. 2013; Zhu et al 2020). Oxidation yield differences have been also identified among different fabrication procedures of UO_2 pellets: 14% for Westinghouse UO_2 pellet (Nilsson et al. 2011) and 6% for a UO_2 pellet manufactured by hot pressing (Trummer et al. 2008; Pehrman et al. 2012).

Because of the above, a new simulation was run by adjusting the oxidation yield to fit the $[U]$ to the measured concentrations. Figure 14 shows that by considering a yield of 4% for the UO_2 oxidation process with $\cdot OH$, the model can reproduce simultaneously both the experimental U and H_2O_2 concentrations.

5 Concluding remarks

As concluding remarks, the present document includes the following two points summarising the main aspects of the study.

5.1 1D reactive transport model

A 1D reactive transport model has been implemented in iCP (Nardi et al. 2014). The model solves the challenge of coupling the complete water radiolysis system with chemical complexation and dissolution/precipitation reactions. It is worth noting that these processes occur at very different time scales, often with rates differing by more than 6 orders of magnitude. This model was calibrated using experimental data (Riba et al. 2020).

The model not only integrates the radiolysis of water but also two important systems: uranium (as the main element of the fuel) and the iron of the steel-container and metallic insert. Both systems have a very complex chemistry. Also, the model has the potential to be extended to include other chemical processes involved in the complex system of SF, steel-container and water chemistry. Therefore, the present work represents a step forward towards the development of a robust model to assess the performance and the safety of a DGR for spent nuclear fuel.

The estimated $\text{UO}_2(\text{am,hyd})$ dissolution rate determined from the model without $\text{Fe}(\text{s})$ is $2 \cdot 10^{-6} \text{ y}^{-1}$. Including iron in the model reduced the corrosion rate down to 10^{-6} y^{-1} and $2 \cdot 10^{-7} \text{ y}^{-1}$, with a steel surface zone length of 1 μm and 1 mm, respectively. These matrix dissolution rates are consistent with the values considered in safety assessments (10^{-7} y^{-1} , with maximum of 10^{-6} y^{-1} and minimum of 10^{-8} y^{-1}), when the inhibiting (protecting) effect of H_2 on the long-term dissolution of SF matrix is considered (Martínez Esparza, 2005; SKB, 2010; POSIVA, 2013; Johnson, 2014; NWMO, 2015; JAEA, 2015).

5.2 Effect of metallic dopants on spent fuel dissolution

The effect of the new dopants (Cr and Al) contained in “modern” fuels on the oxidation of the spent fuel matrix has been studied by different partners of DisCo through leaching experiments of irradiated UO_{2+x} and non-irradiated model materials. These studies have quantified and compared the matrix dissolution of the doped and the undoped material. On the other hand, a comprehensive thermodynamic model has been developed in DisCo to predict chemical equilibria and oxygen potentials of Cr-doped and non-doped UO_2 fuels under operation conditions in light water reactors (Curti et al. 2020).

So far, the experimental results from the Cr/Al doped- UO_x spent fuel compared with standard UO_2 spent fuel support the hypothesis that there is no major difference in leaching behaviour of the fuel matrix between the doped and the un-doped fuels (Fidalgo et al. 2020, Nilsson et al. 2017). Note that these results are also consistent with the observations from the leaching experiments from JÜLICH in which only a slightly higher initial dissolution rate is determined for standard UO_2 in comparison with Cr-doped UO_2 pellets. This difference is attributed only to the increase of density due to the chromia doping (Kegler et al., 2020). These experimental findings are in accordance with the modelling study of Curti et al. (2020), which concludes that Cr-doping should have no significant effect on the oxidation state of UO_2 fuels irradiated in light water reactors.

Another interesting remark is derived from the simulation results of the leaching experiments from CIEMAT (section 4.2). The results indicate that when Cr_2O_3 is supported on Al_2O_3 (in the UO_2 doped with 0.05% Cr_2O_3 – 0.02% Al_2O_3), chromia can activate H_2 , having a similar function as the epsilon particles contained in the irradiated spent fuel and, therefore, limiting the pellet matrix dissolution (Carbol et al, 2009; Trummer and Jonsson 2010; Ollila, 2011). This effect is limited or insignificant in the UO_2 doped with Cr_2O_3 in absence of Al_2O_3 .

In the light of these results the model presented in this report can be applied not only to standard UO_x spent fuel but also to Cr/Al doped- UO_x spent fuel.

6 References

- Andra Référentiel matériaux, Tome 4 la corrosion des matériaux métalliques, Andra, Paris, 2005
- Arborelius J, Backman K, Hallstadius L, Limbäck M, Nilsson J, Rebensdorff B, Zhou G, Kitano K, Löffström R, Rönnerberg G (2012). Advanced doped UO_2 pellets in LWR applications, *J. Nucl. Sci. Techn.* 43, 967-976.
- Barreiro Fidalgo, A., Kumagai, Y., Jonsson, M. (2018). The role of surface-bound hydroxyl radicals in the reaction between H_2O_2 and UO_2 . *Journal of Coordination Chemistry*, 71(11-13), 1799-1807.
- Bruno, J., Casas, I., Puigdomènech, I. (1991). The kinetics of dissolution of UO_2 under reducing conditions and the influence of an oxidized surface layer (UO_{2+x}): Application of a continuous flow-through reactor. *Geochimica et Cosmochimica Acta*, 55(3), 647-658.
- Bruno J. and Ewing R.C (2006)., *Spent Nuclear Fuel, Elements*, 2, 343–349.
- Carbol, P. Fors, T.Gouder, K. Spahiu (2009). Hydrogen suppresses UO_2 corrosion. *Geochimica et Cosmochimica Acta* 73 (2009) 4366–4375.
- Cera, E., Bruno, J., Duro, L., Eriksen, T. (2006). Experimental determination and chemical modelling of radiolytic processes at the spent fuel/water interface. SKB TR 06-07, Svensk Kärnbränslehantering AB.
- Cherian, M., Rao, M. S., Yang, W. T., Jehng, J. M., Hirt, A. M., & Deo, G. (2002). Oxidative dehydrogenation of propane over $\text{Cr}_2\text{O}_3/\text{Al}_2\text{O}_3$ and Cr_2O_3 catalysts: effects of loading, precursor and surface area. *Applied Catalysis A: General*, 233(1-2), 21-33.
- Christensen, H., Sunder, S., Shoesmith, D. W. (1994). Oxidation of nuclear fuel (UO_2) by the products of water radiolysis: development of a kinetic model. *Journal of alloys and compounds*, 213, 93-99
- Clarens, F., De Pablo, J., Casas, I., Giménez, J., Rovira, M. (2003). Surface Site Densities of Uranium Oxides: UO_2 , U_3O_8 . *MRS Online Proceedings Library*, 807(1), 730-735.
- Cobos, J., Rodríguez-Villagra, N., Fernández, S., Gutierrez, L., Bonales, L.J., Durán, S., Anta, L. (2019) Ongoing CIEMAT activities on fabrication and stability studies of doped UO_2 in the fame of the DisCo project: sample characterization, experimental set-up and first results. In: Evins, L.Z, Valls, A., Duro, L. (2019) 2nd Annual Meeting Proceedings DisCo project (Grant Agreement: 755443).
- COMSOL Multiphysics, <https://www.comsol.com/>.

Cooper, M. W. D., Stanek, C. R., Andersson, D. A. (2018). The role of dopant charge state on defect chemistry and grain growth of doped UO₂. *Acta Materialia*, 150, 403-413.

Duro, L., Riba, O., Martínez-Esparza, A., Bruno, J. (2013). Modelling the activation of H₂ on spent fuel surface and inhibiting effect of UO₂ dissolution. *MRS Proceedings 1518*, 133

Duro, L., Tamayo, A., Bruno, J., Martínez-Esparza A. (2009). Integration of the H₂ inhibition effect of UO₂ matrix dissolution into radiolytic models. *Proceedings of the 12th International Conference on Environmental Remediation and Radioactive Waste Management. ICEM2009-16239*. October 11-15, 2009, Liverpool, UK.

Ewing, R (2015) Long-term storage of spent nuclear fuel. *Nature Materials* 14, 252–257 doi:10.1038/nmat4226.

Eriksen, T. E., Jonsson, M., Merino, J. (2008). Modelling of time resolved and long contact time dissolution studies of spent nuclear fuel in 10 mM carbonate solution—a comparison between two different models and experimental data. *Journal of Nuclear Materials*, 375(3), 331-339.

Féron, D., Crusset, D., Gras, J. M. (2008). Corrosion issues in nuclear waste disposal. *Journal of Nuclear Materials*, 379(1-3), 16-23.

Fidalgo, A. B., Roth, O., Puranen, A., Evins, L. Z., and Spahiu, K. (2020) Aqueous leaching of ADOPT and standard UO₂ spent nuclear fuel under H₂ atmosphere. *MRS Advances* © 2020 Materials Research Society. DOI: 10.1557/adv.2020.69.

Giffaut, E., Grivé, M., Blanc, Ph., Vieillard, Ph., Colàs, E., Gailhanou, H., Gaboreau, S., Marty, N., Madé, B., Duro, L. (2014). Andra thermodynamic database for performance assessment: ThermoChimie. *Applied Geochemistry* 49, 225-236.

Grambow, B., Bruno, J., Duro, L., Merino, J., Tamayo, A., Martin, C., Pepin, G., Schumacher, S., Smidt, O., Ferry, C., Jegou, C., Quiñones, J., Iglesias, E., Villagra, N.R., Nieto, J.M., Martínez-Esparza, A., Loida, A., Metz, V., Kienzler, B., Bracke, G., Pellegrini, D., Mathieu, G., Wasselin-Trupin, V., Serres, C., Wegen, D., Jonsson, M., Johnson, L., Lemmens, K., Liu, J., Spahiu, K., Ekeroth, E., Casas, I., de Pablo, J., Watson, C., Robinson, P. and Hodgkinson, D. (2010). MICADO (Model uncertainty for the mechanism of dissolution of spent fuel in nuclear waste repository). Final report.

He H, Keech PG, Broczkowski ME, Noël JJ, Shoesmith DW (2007). Characterization of the influence of fission product doping on the anodic reactivity of uranium dioxide. *Canadian Journal of Chemistry*, 85(10): 702-713.

IAEA (2010). *Advanced Fuel Pellet Materials and Fuel Rod Design for Water Cooled Reactors*. IAEA TECDOC No. 1654. INTERNATIONAL ATOMIC ENERGY AGENCY VIENNA.

Iglesias, E., Quiñones, J. (2008). Analogous materials for studying spent nuclear fuel: The influence of particle size distribution on the specific surface area of irradiated nuclear fuel. *Applied surface science*, 254(21), 6890-6896.

JAEA (2015). Preliminary Assessment of Geological Disposal System for Spent Fuel in Japan - First Progress Report on Direct Disposal. JAEA-Research, 2015-016.

Jerden, J. L., Frey, K., Ebert, W. (2015). A multiphase interfacial model for the dissolution of spent nuclear fuel. *Journal of Nuclear Materials*, 462, 135-146.

Jibril, B. Y., Elbashir, N. O., Al-Zahrani, S. M., Abasaed, A. E. (2005). Oxidative dehydrogenation of isobutane on chromium oxide-based catalyst. *Chemical Engineering and Processing: Process Intensification*, 44(8), 835-840.

Jonsson, M., Ekeröth, E., & Roth, O. (2003). Dissolution of UO₂ by one-and two-electron oxidants. *MRS Online Proceedings Library*, 807(1), 277-282.

Johnson, L., (2014). A model for radionuclide release from spent UO₂ and MOX fuel. NAB 13-37.

Józwiak, W. K. and Dalla Lana, I. G. (1997). Interactions between the chromium oxide phase and support surface; redispersion of α -chromia on silica, alumina and magnesia. *Journal of the Chemical Society, Faraday Transactions*, 93(15), 2583-2589.

Kelm, M., Bohnert, E. (2004) A kinetic model for the radiolysis of chloride brine, its sensitivity against model parameters and a comparison with experiments, *Forschungszentrum Karlsruhe, FZKA 6977*.

Kegler, P., Klinkenberg, M., Bukaemskiy, A., Brandt, F., Deissmann, G., Bosbach, D. (2020) Chromium doped UO₂-based Model Systems: Synthesis and Characterization of Model Materials for the Study of the Matrix Corrosion of Spent Modern Nuclear Fuels. In: Evins, L.Z, Valls, A., Duro, L. (2020) 3rd Annual Meeting Proceedings DisCo project (Grant Agreement: 755443).

Kirkegaard, P., Bjergbakke, E. (2002). CHEMSIMUL: a simulator for chemical kinetics. Roskilde, Denmark: Riso National Laboratory, Riso-R-1085(EN).

Lousada, C. M., Trummer, M., Jonsson, M. (2013). Reactivity of H₂O₂ towards different UO₂-based materials: The relative impact of radiolysis products revisited. *Journal of nuclear materials*, 434(1-3), 434-439.

Martínez Esparza, A., Cera, E., Andriambololona, Z., Bruno, J., Casas, I., Clarens, F., ... & Spahiu, K. (1998). D12. Conceptual model of the Matrix Alteration Model (MAM). WP4: Matrix Model Construction. Contract N° FIKWCT-2001-20192 SFS. In A. Martínez Esparza, and E. Cera, Eds. European Commission. 5th Euratom Framework Programme, 2002, 63.

Martínez Esparza, A., Cuñado, M. A., Gago, J. A., Quiñones, J., Iglesias, E., Cobos, J., González de la Huebra, A., Cera, E., Merino, J., Bruno, J., de Pablo, J., Casas, I., Clarens, F., Giménez, J. (2005). Development of a Matrix Alteration Model (MAM), ENRESA PT-01-2005.

Merino, J., Cera, E., Bruno, J., Quinones, J., Casas, I., Clarens, F., ... & Martínez-Esparza, A. (2005). Radiolytic modelling of spent fuel oxidative dissolution mechanism. Calibration against UO_2 dynamic leaching experiments. *Journal of nuclear materials*, 346(1), 40-47

Nardi, A., Idiart, A., Trincherro, P., de Vries, L. M., and J. Molinero (2014). Interface COMSOL-PHREEQC (iCP), an efficient numerical framework for the solution of coupled multiphysics and geochemistry. *Computers & Geosciences* 69: 10-21.

Nilsson, S., and Jonsson, M. (2011). H_2O_2 and radiation induced dissolution of UO_2 and SIMFUEL pellets. *Journal of Nuclear Materials*, 410(1-3), 89-93.

Nilsson, K., Roth, O., Jonsson, M. (2017). Oxidative dissolution of ADOPT compared to standard UO_2 fuel. *Journal of Nuclear Materials*, 488, 123-128.

NWMO (2015). Technical Program for Long-Term Management of Canada's Used Nuclear Fuel – Annual Report 2014. NWMO TR-2015-01.

Ollila K (2011). Influence of Radiolysis on UO_2 Fuel Matrix Dissolution Under Disposal Conditions - Literature Study. Posiva Working Report 2011-27, 64 pp. Posiva Oy, Olkiluoto, Finland.

Parkhurst, D. L., and C. A. J. Appelo (2013) Description of input and examples for PHREEQC version 3—A computer program for speciation, batch-reaction, one-dimensional transport, and inverse geochemical calculations, U.S. Geological Survey Techniques and Methods, book 6, chap. A43, 497 p.

Pehrman, R., Trummer, M., Lousada, C. M., Jonsson, M. (2012). On the redox reactivity of doped UO_2 pellets—Influence of dopants on the H_2O_2 decomposition mechanism. *Journal of Nuclear Materials*, 430(1-3), 6-11.

Poinsot, C., Cowper, M., Grambow, B., Cavedon, J.M., McMennamin, T. (2004) in: EURADWASTE '04, 29–31 March 2004, Luxembourg.

POSIVA (2013). Safety Case for the Disposal of Spent Nuclear Fuel at Olkiluoto - Models and Data for the Repository System 2012. POSIVA 2013-01.

Odorowski, M., (2015). Etude de l'altération de la matrice $(\text{U,Pu})\text{O}_2$ du combustible irradié en conditions de stockage géologique : Approche expérimentale et modélisation géochimique. Doctoral Thesis.

Odorowski, M., Jégou, Ch., de Windt, L., Broudic, V., Jouan, G., Peugeot, S., Martin, Ch., (2017). Effect of metallic iron on the oxidative dissolution of UO_2 doped with a radioactive alpha emitter in synthetic Callovian-Oxfordian groundwater. *Geochimica et Cosmochimica Acta*, 219.

Puigdomenech, I et al (2001). O_2 depletion in granitic media. SKB TR-01-05, Svensk Kärnbränslehantering AB.

Raiko (2012). Canister design 2012. Posiva Report 2012-13.

Razdan M & Shoesmith DW (2014): Influence of Trivalent-Dopants on the Structural and Electrochemical Properties of Uranium Dioxide (UO₂) Journal of The Electrochemical Society, 161 (3) H105-H113.

Riba, O., Coene, E., Silva, O., Duro, L. (2020). Spent fuel alteration model integrating processes of different time-scales. MRS Advances, 5(3), 159-166.

Rodríguez-Villagra, N., Fernández, S., Jiménez-Bonales, L., Milena-Pérez, A., Núñez, A., Durán, S., Anta, L., Gutiérrez, L., Cobos, J. (2020) Production of unirradiated advanced doped UO₂ fuel for dissolution studies at repository conditions. In: Evins, L.Z, Valls, A., Duro, L. (2020) 3rd Annual Meeting Proceedings DisCo project (Grant Agreement: 755443).

Rodríguez-Villagra, N., Durán, S., Cobo, J. M., Serrano, L., Missana, T., Cobos, J. (2016) "Densidad de sitios superficiales y capacidad de sorción de la matriz de combustible irradiado, UO₂," CIEMAT2016.

Rodríguez-Villagra, N., Serrano, L., Durán, S., Cobos, J., Quiñones, J. (2017) Estudios de alteración y modelación de la matriz del combustible nuclear irradiado en condiciones reductoras y a diferente fuerza iónica., CIEMAT2017.

Romero, E., Rodríguez, J. C., Peña, J.A., Monzón A. (1996) Coking Kinetics of a Cr₂O₃/Al₂O₃ Catalyst During 1 -Butene Dehydrogenation: Effect of H₂, Partial Pressure. The Canadian Journal of Chemical Engineering, Vol. 74.

Roth, O., Puranen, A., Askeljung, C., and Cui, D. (2014). Selection of materials and characterization of samples used in spent fuel leaching and laser ablation studies. In: Kienzler, B., Metz, V., Duro, L., Valls, A. (2014) Final (3rd) Annual Workshop Proceedings. FIRST-Nuclides project (Contract Number: 295722).

Scharf, U., Schneider, H., Baiker, A., & Wokaun, A. (1994). Chromia supported on titania. III. structure and spectroscopic properties. Journal of Catalysis, 145(2), 464-478.

Shoesmith, D. (2013) Chemistry/electrochemistry of spent nuclear fuel as a wasteform. In Burns & Sigmon (Eds.) Uranium - Cradle to Grave. Mineralogical Association of Canada Short Course Series volume 43, 437pp. Mineralogical Association of Canada, Canada.

Smart, N.R. and Hoch, A.R. (2010). A survey of steel and Zircaloy corrosion data for use in the SMOGG gas generation model, Serco Report SA/ENV-0841, Issue 3.

Sohn, J. R. and Ryu, S. G. (1993). Surface characterization of chromium oxide-zirconia catalyst. Langmuir, 9(1), 126-131.

Svensk Kärnbränslehantering AB (2010). Data report for safety assessment SR-Site . SKB TR-10-52.

ThermoChimie Database version 9b0. Thermodynamic database for performance assessment. Consortium Andra - Ondraf/Niras - RWM. <https://www.thermochimie-tdb.com/>. Giffaut, E., Grivé, M., Blanc, Ph., Vieillard, Ph., Colàs, E., Gailhanou, H., Gaboreau, S., Marty, N., Madé,

- B., Duro, L. (2014). Andra thermodynamic database for performance assessment: ThermoChimie. *Applied Geochemistry* 49, 225-236.
- Tian, Z., Jiang, S. B., Jia, X. (2017). Accelerated Monte Carlo simulation on the chemical stage in water radiolysis using GPU. *Physics in Medicine & Biology*, 62(8), 3081.
- Trummer, M., Dahlgren, B., Jonsson, M. (2010). The effect of Y_2O_3 on the dynamics of oxidative dissolution of UO_2 . *Journal of Nuclear Materials*, 407(3), 195-199.
- Trummer, T., M. Jonsson M, J. (2010). Resolving the H_2 effect on radiation induced dissolution of UO_2 -based spent nuclear fuel *Nucl. Mater.*, 396, 163–169.
- Trummer, M., Nilsson, S., Jonsson, M. (2008). On the effects of fission product noble metal inclusions on the kinetics of radiation induced dissolution of spent nuclear fuel. *Journal of Nuclear Materials*, 378(1), 55-59.
- Wu, L., Beauregard, Y., Qin, Z., Rohani, S., Shoesmith, D. W. (2012). A model for the influence of steel corrosion products on nuclear fuel corrosion under permanent disposal conditions. *Corrosion Science*, 61, 83-91.
- Wu, L., Liu, N., Qin, Z., Shoesmith, D.W. (2014a). Modeling the radiolytic corrosion of fractured nuclear fuel under permanent disposal conditions. *Journal of The Electrochemical Society*, 161(8), E3259-E3266.
- Wu, L., Qin, Z., Shoesmith, D. W. (2014b). An improved model for the corrosion of used nuclear fuel inside a failed waste container under permanent disposal conditions. *Corrosion Science*, 84, 85-95.
- Zetterström Evins, L., Juhola, P., Vähänen, M. (Eds.) (2014). REDUPP Final Report. POSIVA report 2014-12.1. 128 pp. <http://www.posiva.fi/files/3672/WR2014-12.1.pdf>.
- Zaki, M. I., Hasan, M. A., Fouad, N. E. (1998). Stability of surface chromate—A physicochemical investigation in relevance to environmental reservations about calcined chromia catalysts. *Applied Catalysis A: General*, 171(2), 315-324.
- Zhu, Z., Noël, J. J., Shoesmith, D. W. (2020). Hydrogen peroxide decomposition on simulated nuclear fuel bicarbonate/carbonate solutions. *Electrochimica Acta*, 340, 135980.

Appendix A

Kinetic reaction scheme¹ for water radiolysis (Kelm and Bohnert, 2004).

Reactions	$M^{-1}\cdot s^{-1}$ or s^{-1}	Reactions	$M^{-1}\cdot s^{-1}$ or s^{-1}
$H_2O \rightarrow H^+ + OH^-$	$k = 2.60E-05$	$H + O_2^- \rightarrow HO_2^-$	$k = 2.00E+10$
$H^+ + OH^- \rightarrow H_2O$	$k = 1.43E+11$	$H + HO_2 \rightarrow H_2O_2$	$k = 8.50E+09$
$H_2O_2 \rightarrow H^+ + HO_2^-$	$k = 3.56E-02$	$H + H_2O_2 \rightarrow H_2O + OH$	$k = 4.20E+07$
$H^+ + HO_2^- \rightarrow H_2O_2$	$k = 2.00E+10$	$H + O_2 \rightarrow HO_2$	$k = 2.10E+10$
$E^- + H_2O \rightarrow H + OH^-$	$k = 1.90E+01$	$HO_2 + HO_2 \rightarrow H_2O_2 + O_2$	$k = 8.40E+05$
$H + OH^- \rightarrow E^- + H_2O$	$k = 2.20E+07$	$HO_2 + O_2^- \rightarrow O_2 + HO_2^-$	$k = 9.60E+07$
$OH + OH^- \rightarrow H_2O + O^-$	$k = 1.30E+10$	$OH + O^- \rightarrow HO_2^-$	$k = 1.80E+10$
$O^- + H_2O \rightarrow OH + OH^-$	$k = 1.80E+06$	$O + O \rightarrow O_2$	$k = 1.00E+09$
$HO_2 \rightarrow H + O_2^-$	$k = 8.00E+05$	$H_2O_2 \rightarrow H_2O + O$	$k = 3.80E-04$
$H + O_2^- \rightarrow HO_2$	$k = 5.00E+10$		
$E^- + H^+ \rightarrow H$	$k = 2.30E+10$		
$E^- + E^- \rightarrow H_2 + OH^- + OH^-$	$k = 5.50E+09$		
$E^- + H \rightarrow H_2 + OH^-$	$k = 2.50E+10$		
$E^- + O_2^- \rightarrow HO_2^- + OH^-$	$k = 1.30E+10$		
$E^- + HO_2 \rightarrow HO_2^-$	$k = 2.00E+10$		
$E^- + H_2O_2 \rightarrow OH + OH^-$	$k = 1.10E+10$		
$E^- + O_2 \rightarrow O_2^-$	$k = 1.90E+10$		
$E^- + HO_2^- \rightarrow O^- + OH^-$	$k = 3.50E+09$		
$OH + OH \rightarrow H_2O_2$	$k = 5.50E+09$		
$OH + E^- \rightarrow OH^-$	$k = 3.00E+10$		
$OH + H \rightarrow H_2O$	$k = 9.70E+09$		
$OH + HO_2 \rightarrow H_2O + O_2$	$k = 6.60E+09$		
$OH + O_2^- \rightarrow O_2 + OH^-$	$k = 1.00E+10$		
$OH + H_2O_2 \rightarrow HO_2 + H_2O$	$k = 2.70E+07$		
$OH + H_2 \rightarrow H + H_2O$	$k = 3.40E+07$		
$OH + HO_2^- \rightarrow HO_2 + OH^-$	$k = 7.50E+09$		
$H + H \rightarrow H_2$	$k = 7.80E+09$		

¹ The kinetic constant for the decomposition reaction of H_2O_2 : $H_2O_2 \rightarrow O + H_2O$ is $k = 1E^{-3} s^{-1}$ (Kelm and Bohnert, 2004, Christensen et al., 1994). As described in Christensen et al. (1994) this rate constant value was set as arbitrary. In the present work, it has been adjusted with the experimental data from Cera et al. (2006) to $3.8E^{-4} s^{-1}$.

Yields of primary products (mol·l⁻¹ x 10⁷) formed on radiolysis of water.

<i>Species</i>	<i>Alpha</i> <i>(Kelm and Bohnert, 2004)</i>	<i>Beta</i> <i>(Eriksen et al. 2008)</i>
G(H ₂ O ₂)	= 0.98	= 0.74
G(HO ₂)	= 0.22	= 0.00
G(H ₂)	= 1.30	= 0.45
G(H)	= 0.21	= 0.60
G(E ⁻)	= 0.06	= 2.80
G(OH)	= 0.25	= 2.80
G(OH ⁻)	= 0.00	= 0.00
G(H ⁺)	= 0.06	= 2.80
G(H ₂ O)	= -2.65	= -4.30

